Discovery of the first quadruple gravitationsally lensed quasar candidate with Pan-STARRS

C. T. Berghea[1], G. Nelson[1], C. E. Rusu[2], C. R. Keeton[3], R. P. Dudik[1]

ciprian.t.berghea@navy.mil

Received _____; accepted _____

[1]U.S. Naval Observatory (USNO), 3450 Massachusetts Avenue NW, Washington, DC 20392, USA

[2]Department of Physics, University of California, Davis, CA 95616, USA

[3]Rutgers, the State University of New Jersey, 136 Frelinghuysen Road, Piscataway, NJ 08854, USA

ABSTRACT

We report the serendipitous discovery of the first quadruple gravitational lens candidate in the Pan-STARRS images. The lensing galaxy is detected by fitting the lens in i, z and y bands using the Hostlens software. There are small differences in the colors of the four quasars images but they are generally consistent quasar at about z $\sim$ 2.6 based on photometric redshift estimates. The lensing galaxy is very faint but we used galaxy templates to estimate z $\sim$ 0.6. We model the lens with both an isothermal ellipsoid (SIE) or a isothermal sphere with shear. While both models provide relatively good fits to the data, there are important discrepancies in the fluxes, especially betwen the B and C components which the models predict should show similar fluxes. These can be explained by differential extinction, microlensing by stars and millilensing due to the dark matter substructure.

Subject headings: black hole physics — galaxies: individual (Holmberg IX) — X-rays: binaries

1. INTRODUCTION

In this letter we report the serendipitous discovery of a quad quasar lens candidate in the Pan-STARRS released images. To our knowledge this is the first gravitational lens discovered in the PS1 data. There are very few known quad lenses and therefore they are very valuable. We provide good evidence for a gravitational lens even without redshift measurements (due to its position it is out of sight until the end of the year).

The prototype Panoramic Survey Telescope and Rapid Response System (Pan-STARRS1, hereafter PS1) is a wide-field imaging system, with a 1.8 m telescope and 7.7 deg^2 field of view, located on the summit of Haleakala in the Hawaiian island of Maui. The first PS1 data was release in December 2016 including both images and photometry (see Chambers et al. 2016). The 1.4 Gpixel camera consists of 60 CCDs with pixel size of 0.256 arcsec (Onaka & al. 2008; Tonry & Onaka 2008). It uses five filters (g_{P1}, r_{P1}, i_{P1}, z_{P1}, y_{P1}), similar to the ones used by the Sloan Digital Sky Survey (SDSS York et al. 2000). The largest survey PS1 performs is the 3π survey, covering the entire sky north of -30 deg declination. Given the large sky coverage and excellent resolution PS1 is expected to reveal nearly 2000 new gravitationally lensed quasars of which about 300 will be quad lensed quasars (Oguri & Marshall 2010).

The lens is very similar to the well studied quad lens RX J1131-1231 (Sluse et al. 2003). At z=0.658 it is one of the nearest known lensed quasars, the three brighter images of the lensed quasar are separated by 1 arcsec, and the fainter image is 3 arcsec away. The quasar images are however fainter by two magnitudes compared to ours (Sluse et al. 2006), but with similar flux discrepancies predicted compared with the models. Sluse et al. (2008) showed that these flux discrepancies can be explained by microlensing. The importance of such quasars is illustrated by the wealth of science this lens has provided over the years. Due to magnification, Reis et al. (2014) were able to measure the black hole spin in this

quasar based on reflection features in X-ray spectra, which has important implications for studies of galaxy evolution. High resolution Hubbble images allowed Brewer & Lewis (2008) to use source reconstruction to resolve the quasar host galaxy and reveal its structure. We hope this new lens will provide a similarly important results in the near future and in this letter we present results based solely on the PS1 data.

In Section 2 we present the results from relative astrometry, photometry and photometric redshift estimates. In Section 3 we model the lens with the gravlens software. Discussion and conclusion are finally presented in Section 4.

2. ASTROMETRY, PHOTOMETRY AND PHOTOMETRIC REDSHIFT

We used the stacked images from PS1 in all five filters to obtain astrometry and photometry using the Hostlens sowftware. The PS1 images (Fig. 1) strongly suggest that the lensed object is a quasar and the photometry results presented in this letter are consistent with this scenario. Therefore we assume that the four PS1 images are quasar images and we fit an analytical PSF model for the quasar for all the five bands. After subtracting the quasar images we detect a faint source in the i, z and y bands, which we believe is the lensing galaxy (Fig. 4)

Here some details on Hostlens and the fits

From the Hostlens fits we calculate absolute photometry and relative astrometry for all images. The measure magnitudes are corrected for extinction using the extinction maps of Schlafly & Finkbeiner (2011).

This has to be changed to use Le Phare method To calculate photometric redshift we used the method of Wu & Jia (2010), which is based on Sloan Digital Sky survey (SDSS) colors. PS1 bands are similar but not identical to the SDSS bands and we

used the corrections of (Finkbeiner et al. 2016) to obtain magnitudes in the SDSS system. Folowing Wu & Jia (2010) we minimize χ^2 to obtain redshits for each of the sources. We plot χ^2_ν in Figure 2 for each quasar image and also fitting all togehter. In the latter case we obtain the best fit at z $\sim$ 0.83, but this is not well constrained, the 1 σ confidence level is (0.625, 2.875). We note that there is a second minimum at z $\sim$ 2.6. χ^2_ν is 0.56 and 1.07 for the two minima, respectively.

The photometric, astrometric and redshift results are summarized in Table 1.

Due to blending of A, B and C components, both Gaia (Gaia Collaboration et al. 2016) and PS1 catalogs identified sources A and D only. PS1 psf magnitudes for A are in general smaller than what we obtained probably due to blending, but for D they are very similar to our uncorrected magnitudes: 18.599±0.013, 18.153±0.002, 18.079±0.007, 17.843±0.0093, 17.534±0.023. Gaia G magnitudes are 15.17 and 18.13 for A and D, respectively. We will use the Gaia position for component D as absolute astrometric reference position for our lens: 26.7923069811, 46.5112731937. The errors for this position are 15.6 and 8.9 mas, respectively.

The lens is also bright in infrared, the unresolved WISE magnitudes for the lens are: 11.524±0.022, 10.434±0.020, 6.769±0.015 ,4.518±0.023 in the WISE bands − W1, W2, W3 and W4, respectively. The WISE colors match very well those of quasars at low redshift (e.g. Mateos et al. 2012).

Finally, the lens is very likely a radio source. The NRAO VLA Sky Survey (NVSS) images show a source at the lens position, 2MASX J01471020+4630433 has a flux of 12.6 mJy at 1.4 GHz. The listed position for this source is only 3 arcsec away from the center of the lens. We are in the process of observing the lens with the Very Large Baseline Array (VLBA).

3. LENS MODELING

We used the gravlens software to model the gravitational lens (Keeton 2001) using the measurements for the g PS1 image We tried two models, Singular Isothermal Ellipsoid (SIE) and a isothermal sphere with shear. The predicted positions and magnitudes are presented in Table 1. In Figure 3 we show lensing critical curves for the two models. The χ^2_ν for these models are 6.0 and 4.9 for these models, respectively. The contribution to residuals is relatively equal from positions and magnitudes for both models.

While the models differ in detail, they are consistent in predicting image brightnesses that differ from what is observed. In particular, the models suggest that the two outer images should be similar in brightness. This is interesting because there are some physical effects that can cause observed image brightnesses to differ from the predictions of simple lens models. Firstly light can be affected as it propagates through the main lens galaxy, for example by differential extinction. This possibility is interesting in light of the color differences between images. Propagation effects tend to be more important at optical wavelengths than at radio wavelengths; this is particularly true of extinction, although there can be scatter broadening at radio wavelengths. Secondly, the light can be affected by stars in the lens galaxy through microlensing. This mainly affects optical wavelengths. Finally, the light can be affected by dark matter substructure in the lens galaxy through millilensing. This could affect all wavelengths.

Measuring the flux ratios in radio with VLBA would provide valuable information that will help us test the lensing hypothesis and understand the various physical effects at play and better constrain the models

4. CONCLUSIONS

The evidence is overwhelming for this to be a lens (configuration reproduced by lensing, similar color for each image, detection of lensing galaxy), but we stop short of claiming that it is a confirmed lens until we get spectroscopy.

The Pan-STARRS1 Surveys (PS1) and the PS1 public science archive have been made possible through contributions by the Institute for Astronomy, the University of Hawaii, the Pan-STARRS Project Office, the Max-Planck Society and its participating institutes, the Max Planck Institute for Astronomy, Heidelberg and the Max Planck Institute for Extraterrestrial Physics, Garching, The Johns Hopkins University, Durham University, the University of Edinburgh, the Queen's University Belfast, the Harvard-Smithsonian Center for Astrophysics, the Las Cumbres Observatory Global Telescope Network Incorporated, the National Central University of Taiwan, the Space Telescope Science Institute, the National Aeronautics and Space Administration under Grant No. NNX08AR22G issued through the Planetary Science Division of the NASA Science Mission Directorate, the National Science Foundation Grant No. AST-1238877, the University of Maryland, Eotvos Lorand University (ELTE), the Los Alamos National Laboratory, and the Gordon and Betty Moore Foundation. This work has made use of data from the European Space Agency (ESA) mission *Gaia* (https://www.cosmos.esa.int/gaia), processed by the *Gaia* Data Processing and Analysis Consortium (DPAC, https://www.cosmos.esa.int/web/gaia/dpac/consortium). Funding for the DPAC has been provided by national institutions, in particular the institutions participating in the *Gaia* Multilateral Agreement.

REFERENCES

Bertin, E., & Arnouts, S. 1996, A&AS, 117, 393

Brewer, B. J., & Lewis, G. F. 2008, MNRAS, 390, 39

Chambers, K. C., Magnier, E. A., Metcalfe, N., et al. 2016, arXiv:1612.05560

Finkbeiner, D. P., Schlafly, E. F., Schlegel, D. J., et al. 2016, ApJ, 822, 66

Gaia Collaboration, Brown, A. G. A., Vallenari, A., et al. 2016, A&A, 595, A2

Keeton, C. R. 2001, arXiv:astro-ph/0102340

Mateos, S., Alonso-Herrero, A., Carrera, F. J., et al. 2012, MNRAS, 426, 3271

Oguri, M., & Marshall, P. J. 2010, MNRAS, 405, 2579

Onaka P., Tonry J. L., Isani S., Lee A., Uyeshiro R., Rae C., Robertson L., Ching G., Proc. 2008, Proc. SPIE, 7014, 12

Peng, C. Y., Ho, L. C., Impey, C. D., & Rix, H.-W. 2010, AJ, 139, 2097

Reis, R. C., Reynolds, M. T., Miller, J. M., & Walton, D. J. 2014, Nature, 507, 207

Schlafly, E. F., & Finkbeiner, D. P. 2011, ApJ, 737, 103

Sluse, D., Surdej, J., Claeskens, J.-F., et al. 2003, A&A, 406, L43

Sluse, D., Claeskens, J.-F., Altieri, B., et al. 2006, A&A, 449, 539

Sluse, D., Eigenbrod, A., Courbin, F., et al. 2008, Manchester Microlensing Conference, 20

Tonry J., Onaka P. 2009, in Ryan S., ed., Proceedings of the Advanced Maui Optical and Space Surveillance Technologies Conference. The Maui Economic Development Board, Kihei, HI, p. E40

Wu, X.-B., & Jia, Z. 2010, MNRAS, 406, 1583

York, D. G., Adelman, J., Anderson, J. E., Jr., et al. 2000, AJ, 120, 1579

Table 1. Lens measurements and modeling results

Property	A	B	C	D	G
Measurements					
g	15.60±0.01	15.72±0.01	16.45±0.02	18.09±0.01	···
r	15.40±0.01	15.55±0.01	16.21±0.01	17.74±0.01	···
i	15.36±0.01	15.57±0.02	16.15±0.02	17.74±0.02	19.50±0.20
z	15.23±0.03	15.50±0.05	16.02±0.01	17.68±0.03	18.95±0.13
y	14.92±0.01	15.23±0.02	15.76±0.02	17.36±0.02	19.20±0.24
Δi	0.0	0.21	0.79	2.38	4.14
Δx	0.000±0.004	-1.185±0.004	1.271±0.005	0.410±0.004	0.240±0.050
Δy	0.000±0.004	-0.441±0.004	-0.074±0.004	-3.310± 0.004	-2.310±0.025
z	0.725	0.825	0.725	0.925	
Model prediction. Isothermal ellipsoid					
Δg	0.0	0.441	0.495	2.565	
Δx	-0.3903	-1.5294	0.9049	0.0	
Δy	3.3137	2.8096	3.0659	0.0	
Model prediction. Isothermal sphere with external shear					
Δg	0.0	0.563	0.617	2.643	
Δx	-0.3863	-1.5378	0.9115	0.0	
Δy	3.2913	2.8116	3.0707	0.0	

Note. — The first four columns are the four quasar images and the fifth column is the lens. The first five rows are magnitude measurements derived using Hostlens and corrected using NED extinction calculator. The following three rows are relative i magnitudes and relative positions in arcseconds averaged between the i and y bands. The next row shows the photometric redshift estimates following Wu & Jia (2010). Following rows shows the model prediction for position and relative magnitudes for two gravitational models.

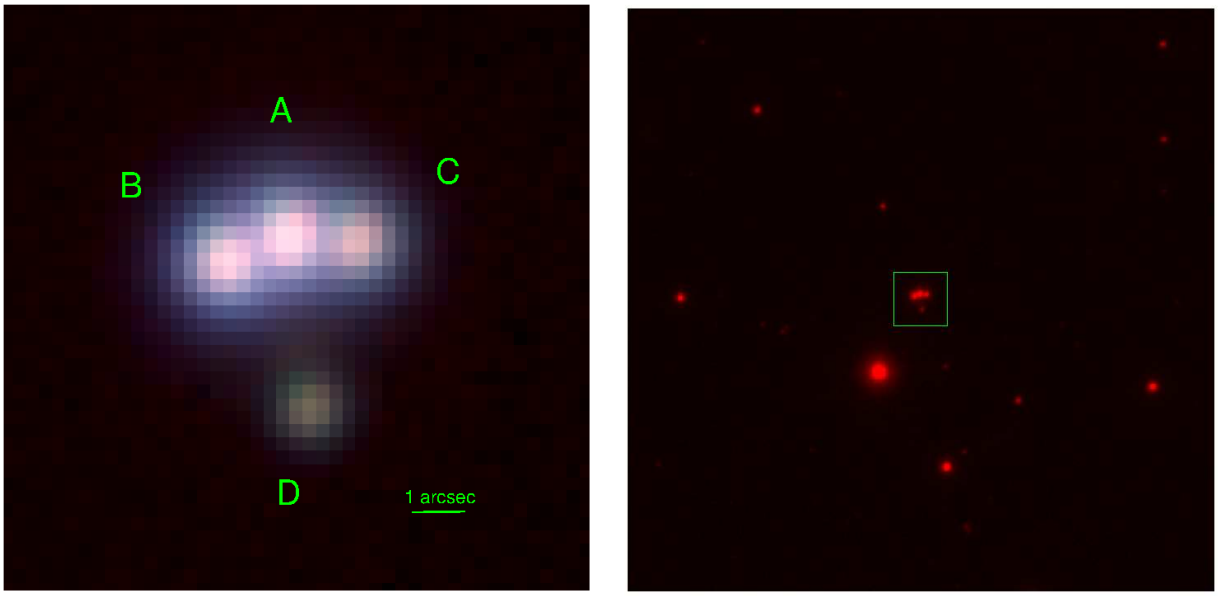

Fig. 1.— PS1 images of the lens candidate. Left: is a color coded close image R-y, G-i, B-g. Right: y image of the surrounding area, image size is 2 arcmin. The bright star south-east of the lens is saturated in the other bands.

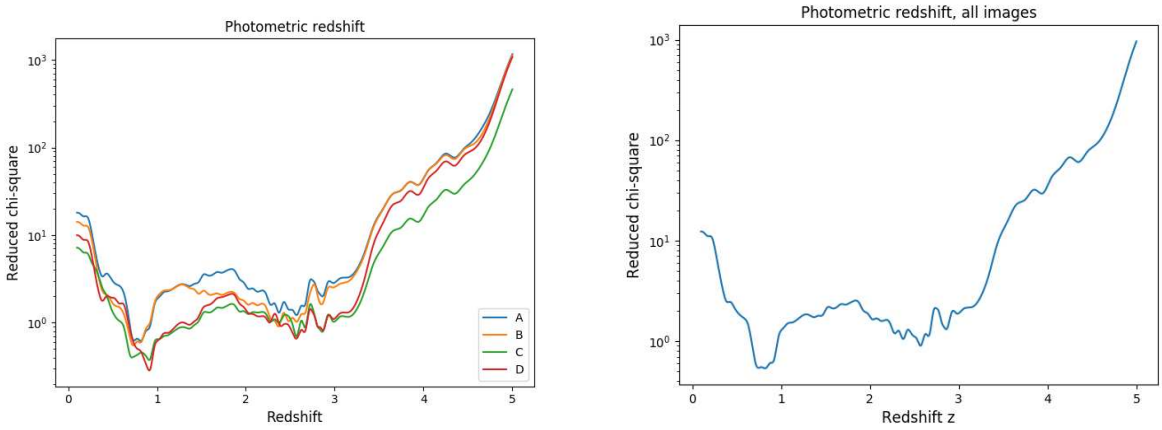

Fig. 2.— Photometric redshift estimates. Left: individually for each image; right: for all images simultanesously

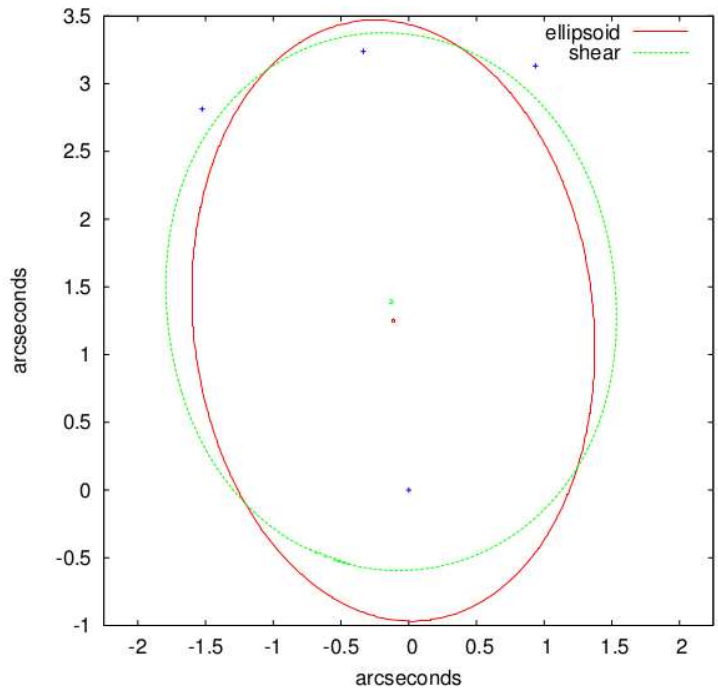

Fig. 3.— Gravitational lens model. Two models were used, isothermal ellipsoid (red) and a isothermal sphere with shear (green). The small circles in the center of the image show the predicted position for the lens galaxy for each model.

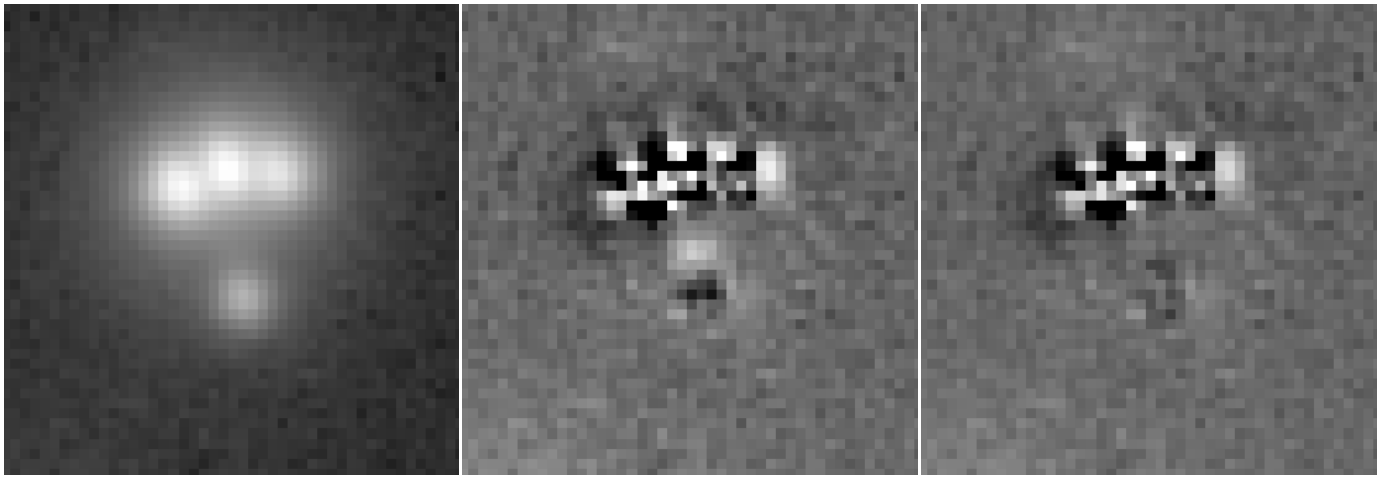

Fig. 4.— Hostlens i band fits. From left to right: the original PS1 image, after the quasar images are removed and finally after the lens image is also removed

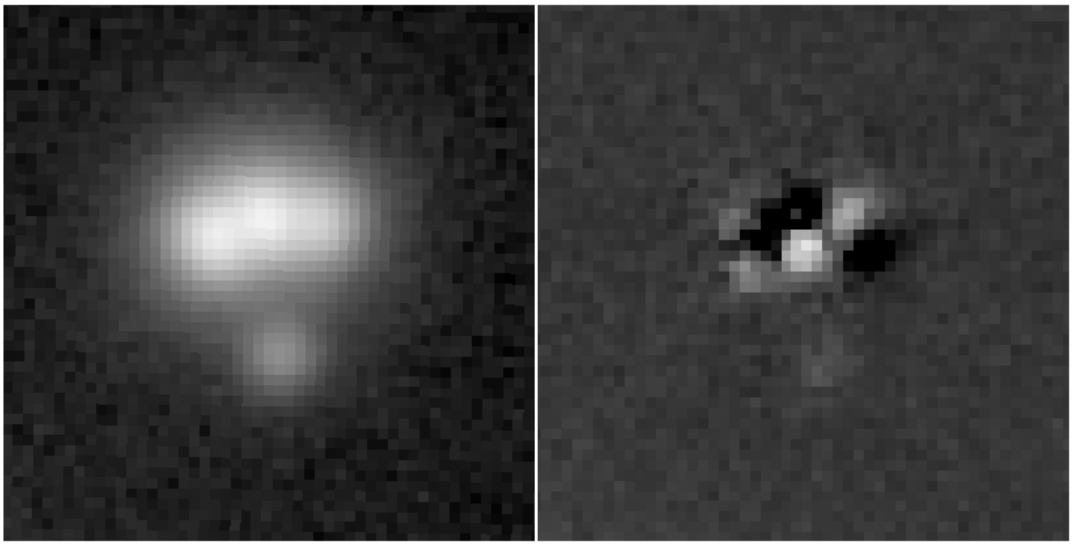

Fig. 5.— Galfit g band for the SIE model

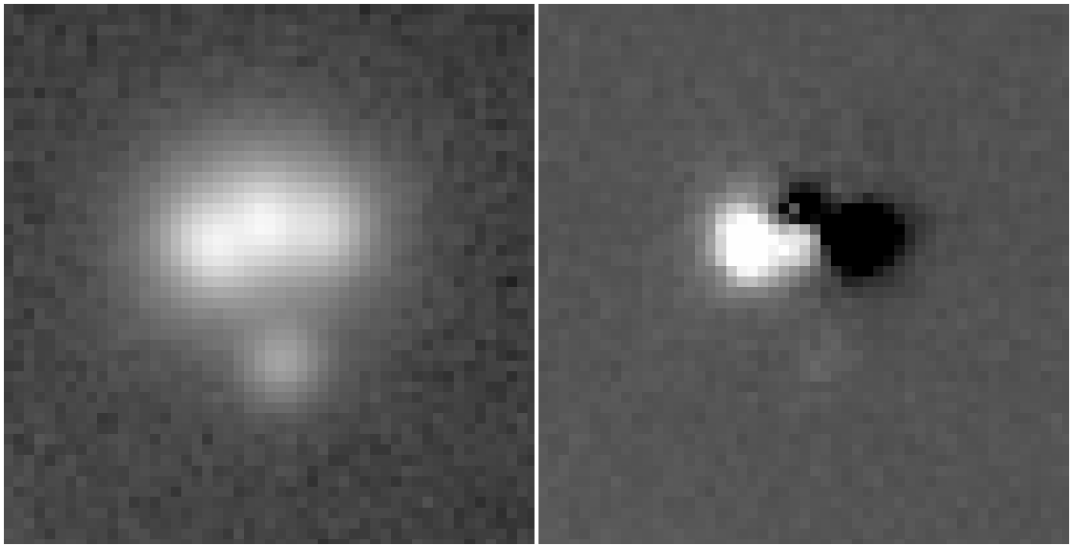

Fig. 6.— Galfit g band for the SIE model with fluxes fixed to the model prediction

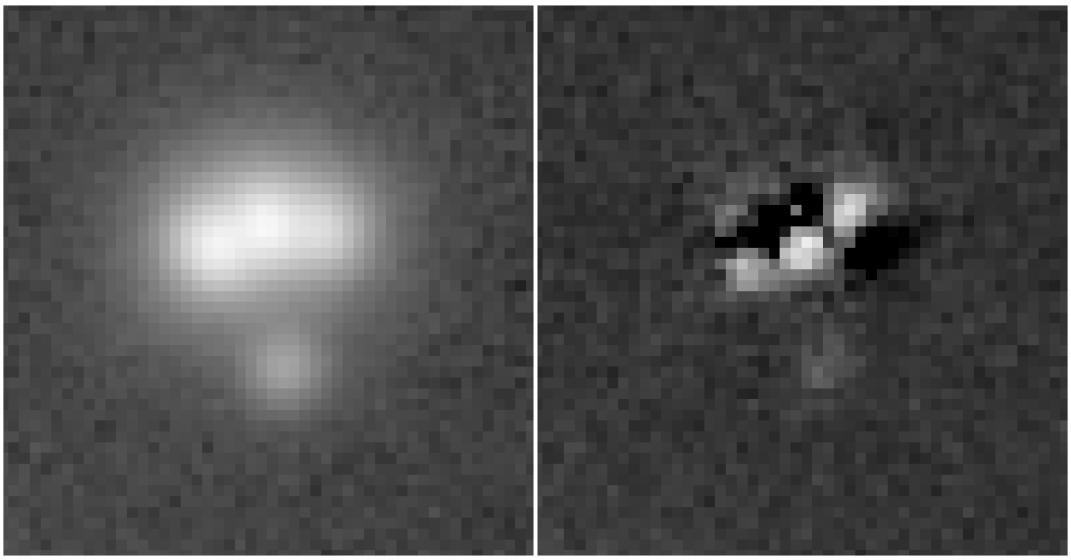

Fig. 7.— Galfit g band for the shear model

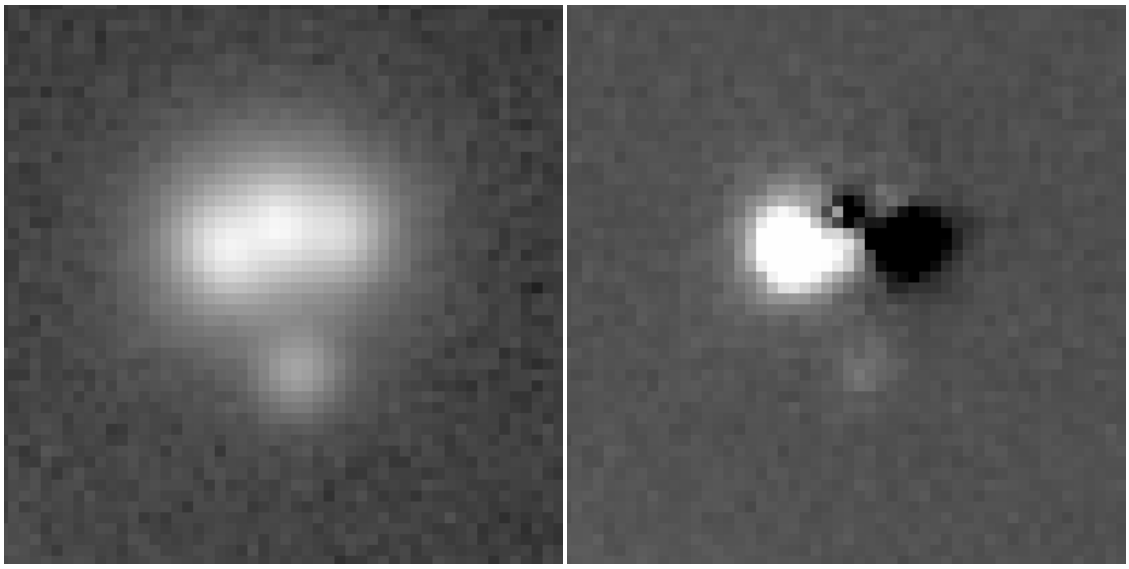

Fig. 8.— Galfit g band for the shear model with fluxes fixed to the model prediction